Access provided by Rutgers University Libraries

Letter

Tuning a circular p–n junction in graphene from quantum confinement to optical guiding

Yuhang Jiang, Jinhai Mao, Dean Moldovan, Massoud Ramezani Masir, Guohong Li, Kenji Watanabe, Takashi Taniguchi, Francois M. Peeters & Eva Y. Andrei

Nature Nanotechnology **12**, 1045–1049 (2017)
doi:10.1038/nnano.2017.181
Download Citation
Condensed-matter physics Electronic properties and materials Physics

Received: 16 January 2017
Accepted: 25 July 2017
Published: 18 September 2017

Abstract

The photon-like propagation of the Dirac electrons in graphene, together with its record-high electronic mobility[1,2,3], can lead to applications based on ultrafast electronic response and low dissipation[4,5,6]. However, the chiral nature of the charge carriers that is responsible for the high mobility also makes it difficult to control their motion and prevents electronic switching. Here, we show how to manipulate the charge carriers by using a circular p–n junction whose size can be continuously tuned from the nanometre to the micrometre scale[7,8]. The junction size is controlled with a dual-gate device consisting of a planar back gate and a point-like top gate made by decorating a scanning tunnelling microscope tip with a gold nanowire. The nanometre-scale junction is defined by a deep potential well created by the tip-induced charge. It traps the Dirac electrons in quantum-confined states, which are the graphene equivalent of the atomic collapse states (ACSs) predicted to occur at supercritically charged nuclei[9,10,11,12,13]. As the junction size increases, the transition to the optical regime is signalled by the emergence of whispering-gallery modes[14,15,16], similar to those observed at the perimeter of acoustic or optical resonators, and by the appearance of a Fabry–Pérot interference pattern[17,18,19,20] for junctions close to a boundary.

Main

In the dual-gate device employed here, the back-gate electrode tunes the global carrier density and the top gate controls local doping under the scanning tunnelling microscope (STM) tip (Fig. 1a). The variable-size p–n junction was realized by controlling the back-gate voltage V_g (Fig. 1b). Before creating the p–n junction we measured the gate dependence of the tunnelling resistance (dI/dV) spectra[21,22] with a pristine Pt–Ir tip, which for low bias voltages (V_b) is known to be non-invasive[22]. By contrast, a strongly biased STM tip can create a potential well that is sufficiently deep to trap electrons in quantum-confined states[10,23]. To access this regime we functionalized the STM tip by gently poking it into a Au electrode to create a large tip–graphene work-function difference, ΔW. The resulting tip-induced potential is controlled by the speed of the tip retraction from the Au electrode. Slow retraction rates (0.1 nm s^{-1}) decorate the tip with a sharp protruding Au nanowire[24,25], while rapid retraction coats it with a Au film (Supplementary Section 2). We evaluated the effect of the tip treatment by comparing the tunnelling spectra before and after the procedure. In Fig. 2 we show the spectra obtained with the sharp nanowire decorated tip (Supplementary Section 3 shows spectra obtained with Au-coated tips and tip calibration). Before tip decoration (Fig. 2a) the spectra exhibit the well-known 'V' shape of unperturbed graphene[22]. The spectra taken with the Au nanowire tip are qualitatively different. In the p-doped regime (Fig. 2b) they feature a resonance peak below the bulk Dirac-point energy (E_D), the energy of which is very sensitive to the global doping level. In the highly p-doped regime ($V_g = -54$ V) the peak appears as a broad and barely distinguishable bump just below the bulk E_D. As doping decreases, it becomes more pronounced and shifts monotonically down in energy, with a second peak emerging at the lowest doping levels, $V_g = -6$ V. The spectra and their gate dependence resemble those of ACSs at supercritically charged impurities in graphene[11,12]. The ACSs are negative-energy states that can bind Dirac electrons to a local charge Z when the interaction strength, $\beta \equiv Z\alpha_g$, exceeds a critical value $\beta_c \approx 0.5$. Here, $\alpha_g = \alpha(c/\kappa v_F)$, where α is the fine-structure constant, c is the speed of light, v_F is the Fermi velocity, and κ is the effective dielectric constant. Similar to the negative-energy resonances observed here, ACSs at supercritically charged vacancies are observed in the p-doped regime only, their energy becomes more negative with reduced carrier density, and for sufficiently large charge and low doping a second resonance appears just below E_D. These similarities suggest that the resonances observed here reflect ACSs associated with the tip-induced local charge[10,23].

Figure 1: Tunable circular p–n junction.

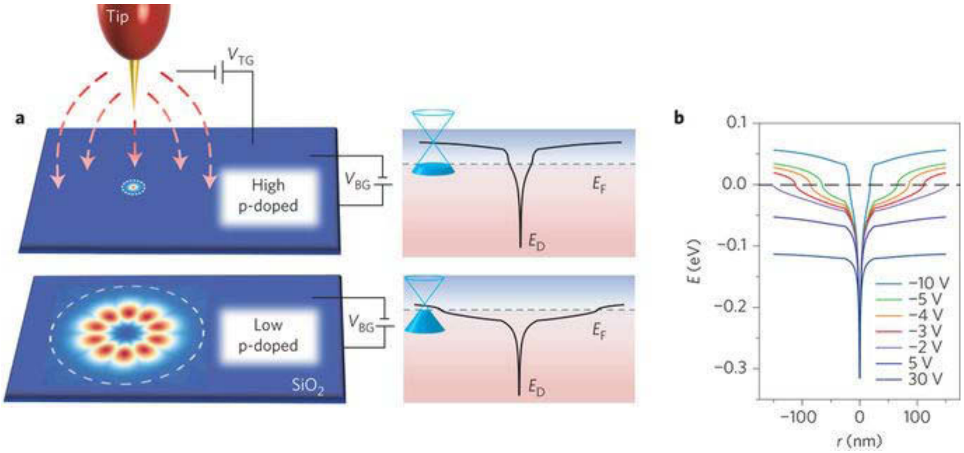

a, Variable-size graphene junctions are produced with a dual-gate configuration consisting of a silicon-substrate back gate (V_{BG}) that controls the global doping level and an STM tip serving as a top gate (V_{TG}) to tune the local carrier concentration under the tip. Top left: nanometre-scale graphene p–n junction created by gating the bulk in the deep p-doped regime. Bottom left: wavefunction distribution for a WGM with angular momentum $m = 10$ supported by a 300 nm junction created in the weakly p-doped regime. Right: back-gate dependence of the tip-induced potential showing the Coulomb-like potential giving rise to the ACS (top) and the cavity-like potential responsible for the WGM (bottom). Dashed line: position of the Fermi level. **b**, Calculated potential profile for a series of back-gate voltages and a tip–graphene work-function difference of $\Delta W = 0.7$ eV.

Figure 2: Gate voltage dependence of the LDOS in a nanoscale graphene p–n junction.

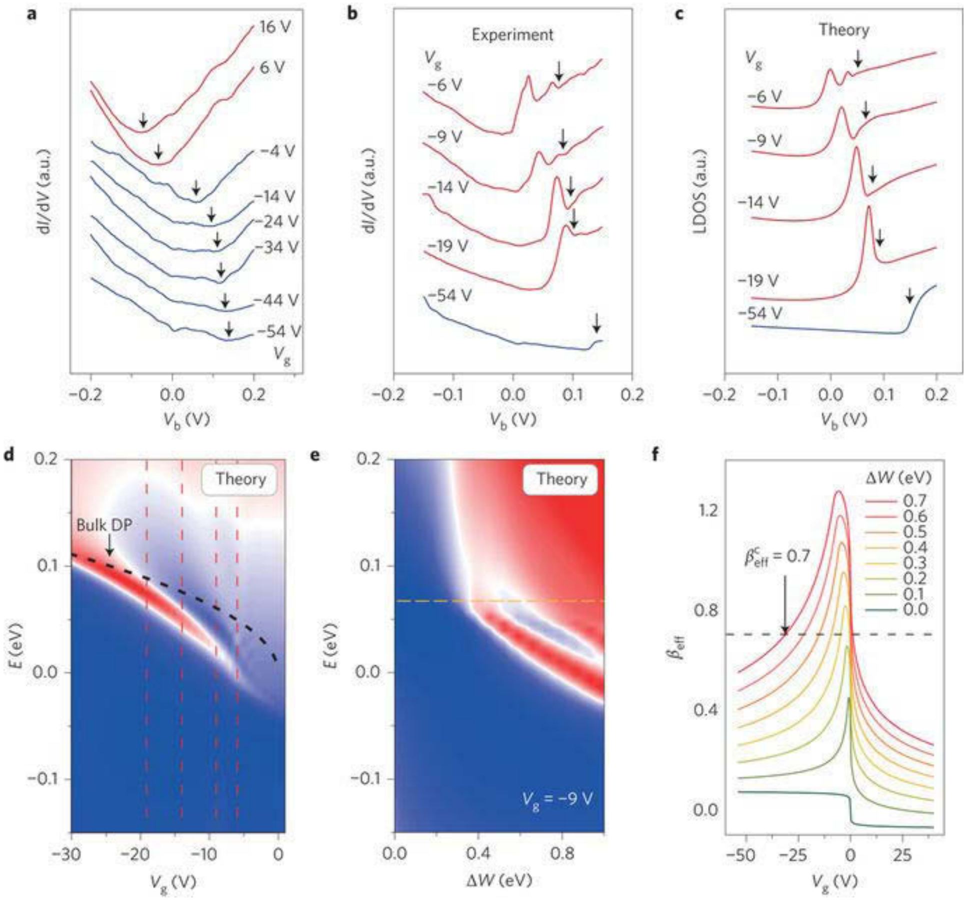

a, Back gate dependence of d*I*/d*V* curves before tip functionalization. **b**, As in **a**, after tip functionalization with a Au nanowire (STM setpoint: V_b = −50 mV, I = 0.1 nA). **c**, Calculated LDOS for the graphene nanojunction for Δ*W* = 0.7 eV. In all panels, arrows indicate bulk E_D. **d**, Two-dimensional map of LDOS evolution with V_g. Dashed curve: evolution of the Dirac-point back-gate voltage. Vertical dashed lines represent curves in **c**. **e**, Two-dimensional map of LDOS evolution with Δ*W*. Dashed line: bulk E_D for V_g = −9 V. **f**, Evolution of β_{eff} with V_g for several values of Δ*W* (as indicated).

To gain insight into these results we calculated the tight-binding local density of states (LDOS) in the presence of the tip, which was modelled as a conical segment that broadens into a spherical shell further away (Supplementary Fig. 6). The tip-induced potential was calculated by using the Thomas–Fermi theory to account for screening (Supplementary Sections 4, 7 and 10). Its evolution with V_b, V_g and tip–graphene work-function difference (ΔW) is shown in Supplementary Figs 4 and 7. The tip-induced potential for a tip with ΔW = 0.7 V is shown in Fig. 1b. With this potential as input, we calculated the gate-voltage dependence of the LDOS (Fig. 2c,d and Supplementary Section 5). The calculated spectra closely match the measured ones: in the highly p-doped regime (V_g = −54 V), there is a broad feature near the bulk E_D; as the carrier concentration decreases (−19 V < V_g < −6 V) a sharp peak appears below E_D that dives into the negative-energy sector and finally a second peak materializes just below E_D. The calculated resonance peak energy strongly depends on ΔW and disappears below a critical value ΔW_c of ~0.3 eV as shown in Fig. 2e. This indicates that, similar to the ACS case, there exists a control parameter, here ΔW, that has to exceed a critical value for the negative-energy resonances to appear. This may not be surprising considering that the sharp tip with its large ΔW creates a deep and narrow potential well that resembles that of a point charge (Fig. 1b). To make the connection with charge-induced ACSs we define an effective point charge which induces the same potential as the tip (Supplementary Section 7). This effective point charge produces an effective interaction strength: $\beta_{eff} = (1/\hbar v_F)\sqrt{(2\int_{r_0}^{R} V(r)^2 r dr/(1 + 2\ln(R/r_0)))}$, where r_0 (~0.25 nm) is a lower cutoff at the scale of a graphene unit cell and R is taken at the crossing between the steep and shallow parts of the potential.

The gate dependence of the calculated β_{eff} for several values of ΔW is shown in Fig. 2f. Compared to the experimental data in Fig. 2b we find that the β_{eff} (V_g) curve with $\Delta W = 0.7$ eV reproduces the observed features. Similar to the data, the curve attains its maximum value for $V_g \approx -6$ V, corresponding to the largest attainable shift of the ACS peak relative to E_D. To determine the critical value, β_{eff}, we note that the resonance peak disappears when it crosses E_D at $V_g \approx -30$ V (Fig. 2d) and that β_{eff} attains supercritical values only for $\Delta W \geq 0.3$ V (Fig. 2e). Both these constraints are satisfied by choosing $\beta_{\mathrm{eff}}^{c} = 0.7$ (dashed line in Fig. 2f). This value is slightly higher than that expected for a pure Coulomb potential, 0.5, which is not surprising given that the tip-induced charge is more spread out than that of a point charge. Furthermore, we find that, similar to the experimental data, β_{eff} increases with reduced carrier density in the p-doped regime and, after peaking, it sharply drops below the critical value upon approaching E_D. These features suggest that the tip-induced negative-energy peaks observed here, similarly to resonances induced by a point charge[10,11,12], can be attributed to atomic collapse physics.

The evolution of the LDOS with junction size is shown in Fig. 3. For $V_g = -14$ V, corresponding to the ACS regime discussed above, the nanometre-size junction traps electrons in a quasi-localized state at its centre (Fig. 3a,e). The crossover to the micrometre-size junction is controlled by tuning V_g to gradually approach the charge neutrality point (CNP). The CNP is defined by the crossing of E_D with the Fermi energy E_F, which is taken as the energy origin. This leads to an increase in screening length, which broadens the top part of the potential well (Fig. 3b,c and Supplementary Section 6). The induced charge spreads out into the circular cavity, the boundaries of which are defined by the sharp kink at the crossing of the potential with E_F (Fig. 1a and Supplementary Fig. 7a). The cavity can form within a narrow range of doping below the CNP. Its radius R_c grows with increasing V_g and diverges at the bulk CNP, beyond which it disappears. In graphene the reflection of electrons at a p–n junction is governed by Klein collimation, which, for certain oblique angles, can produce perfect reflection[3,8]. As a result, the cavity can support whispering-gallery modes (WGMs) when the conditions of total internal reflection and constructive interference are met (Supplementary Section 8). Interestingly, for off-resonance electron energies the junction serves as a lens with tunable focal length that can guide electronic motion[7]. To detect the emergence of WGMs we examined the dI/dV spectra close to the CNP (shown in Fig. 3g). In the figure we observe a succession of nearly equally spaced peaks (red arrows) below the bulk E_D that are consistent with WGMs within the cavity defined by the broad circular p–n junction. This sequence of peak energies clearly does not follow the characteristic $\log E_n \propto n$ of ACS resonances[10,26], excluding their interpretation in terms of high-order ACSs. The evolution of the WGM spectra with gate voltage is shown in Supplementary Fig. 5. Even though the WGMs observed here with the sharp tip are seen only in a narrow doping window, they display the same characteristics as those formed by a blunt Au-coated tip, as shown in Supplementary Figs 4 and 5, and consistent with earlier reports[15]. Tuning the gate voltage into the n-doped regime results in an n^+–n junction (Fig. 3d,h). In this case, with the outer p-doped regime missing, the boundary that sustained WGMs no longer exists and the LDOS becomes featureless. Notably, even though the potential profile has reverted back to the point-charge-like potential, the ACS peak is absent. This can be understood from the doping dependence of β_{eff} (Fig. 2f), which sharply dives below the critical value at the crossing into the n-doped regime[12]. In this regime the circular junction acts as a weak scatterer[7].

Figure 3: LDOS in the variable-size p–n junction.

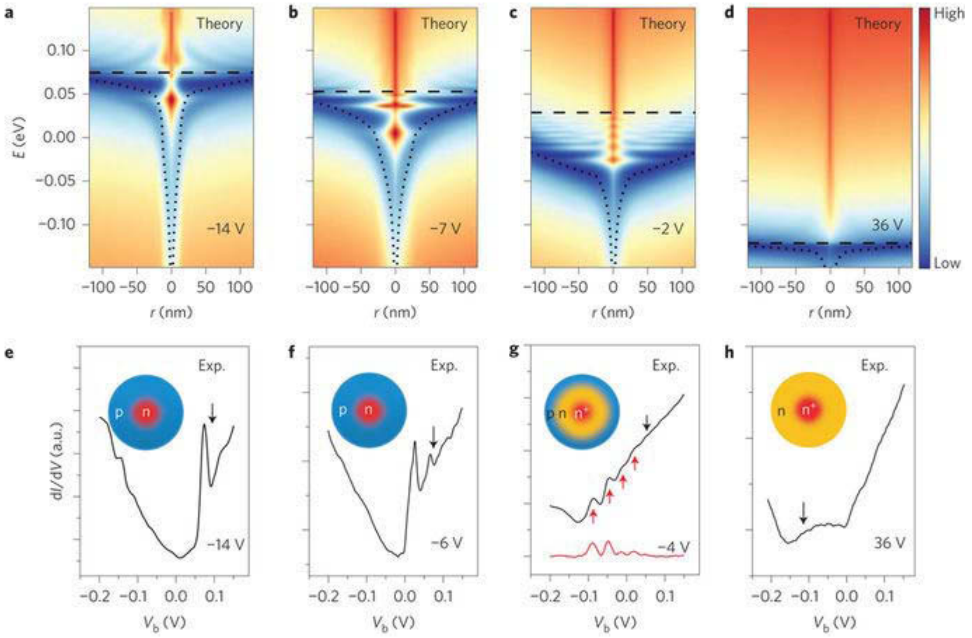

a–d, Simulated map of the LDOS as a function of position relative to the centre of the tip for the indicated back-gate voltages. Dotted lines: potential profile. Dashed lines: the bulk Dirac point. **e–h**, Measured d*I*/d*V* curves for different back-gate voltages corresponding to the simulated maps in **a–d**. Arrows in **g** indicate WGM peaks and the red curve corresponds to the same data after background subtraction. Insets: p–n junction boundaries. Red: highly n-doped regime; yellow: n-doped regime; blue: p-doped regime.

Taking a closer look at the crossover regime where the cavity has almost disappeared (Fig. 3g), we note that the LDOS shows discrete negative-energy modes, $V_b < 0$, corresponding to WGM, while the positive-energy sector, $V_b > 0$, is featureless. The absence of structure for $V_b > 0$ indicates that although the electrons in this regime are weakly scattered by the tip-induced potential[7], the LDOS is unaffected. This situation is changed by placing the tip-induced junction close to a reflecting boundary. The interference of the electron beams trapped between the tip potential and the boundary produces a Fabry–Pérot pattern, which is strongly enhanced at the tip position due to the cavity focusing effect (Supplementary Fig. 9). This produces a sequence of equally spaced positive energy peaks in the LDOS. Their energy separation fits the expression $\Delta E = \pi\hbar v_F/d$, where d is the tip–boundary distance (100.7 nm), as shown by the simulation in Fig. 4a. The data in Fig. 4b reveal the effect of a boundary defined by a Au electrode (Fig. 4c) placed at a distance $d \approx 100$ nm from the junction. We note six equally spaced ($\Delta E \approx 19$ meV) positive energy peaks (above E_D), which are consistent with the generation of Fabry–Pérot interference resulting from reflections off the electrode. The $1/d$ position dependence of the measured peak energy separation agrees with numerical simulations of Fabry–Pérot interference peaks, as shown in the inset to Fig. 4c. Further support for this picture is provided by the disappearance of the positive energy peaks for distances larger than $d \approx 250$ nm, from which we estimate a phase coherence length of ~500 nm in this sample. As in the case of the WGM, the strong Fabry–Pérot interference peaks observed here can be attributed to Klein collimation, which enhances the visibility of the interference pattern[17,27,28].

Figure 4: Fabry–Pérot interference pattern.

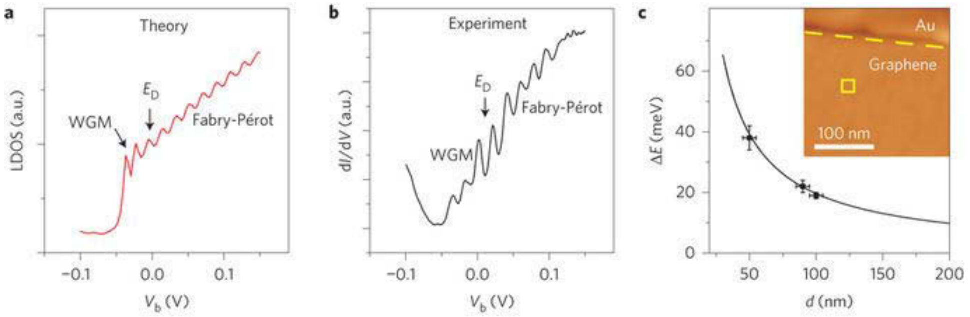

a, Calculated LDOS for the graphene junction showing WGMs and Fabry–Pérot resonances due to reflections from a nearby boundary. E_D in **a** and **b** is the bulk Dirac point. **b**, Measured d*I*/d*V* spectrum at a tip-induced p–n junction for $V_g = -0.6$ V recorded at the position marked by the square in the inset in **c** (STM setpoint: $V_b = -50$ mV, $I = 0.1$ nA, $V_g = -0.6$ V). **c**, Evolution of peak period with distance to the boundary: measured (symbols) and theoretical curve (black line), $\Delta E = \pi\hbar v_F/d$. Horizontal error bars represent uncertainty in the tip–boundary distance. Error bars for Δ*E* reflect uncertainty in peak energies. Inset: STM topography of the graphene sample close to the Au electrode boundary (dashed line).

The creation of tunable p–n junctions demonstrated here, which can straddle the crossover between quantum confinement and optical guiding, paves the way to novel design architectures for electronic transport. For example, devices incorporating graphene nanojunction arrays consisting of nanowires or nanodots with large ΔW deposited on a thin insulating film covering gated graphene could add an important building block to the electron–optics toolbox by enabling both switching and guiding of Dirac electrons.

Methods

The samples consisted of twisted double-layer exfoliated graphene[29,30] deposited on an hBN flake by a dry transfer process[31] (Supplementary Section 1). The hBN flake was exfoliated on a 300 nm SiO_2 dielectric layer capping a highly doped Si substrate serving as back gate. After annealing in forming gas at 300 °C for 3 h, the first graphene layer was transferred onto the hBN with a polymethyl methacrylate/polyvinyl alcohol (PMMA/PVA) sacrificial film, which was subsequently removed by acetone. The second layer was deposited following the same steps. Au/Ti electrodes were then deposited using standard scanning electron microscope lithography followed by overnight annealing. STM measurements are performed in a home-built instrument[32] at 4.2 K using a cut $Pt_{0.8}Ir_{0.2}$ tip, which is known to be non-invasive within the typical range of experimental bias voltages, $V_b < 0.2$ V. dI/dV spectra were collected by the standard lock-in method with a 2 mV, 473.1 Hz modulation added to the d.c. bias. We defined the gate voltage $V_g = V_{BG} - V_0$, as the applied back-gate voltage V_{BG}, measured with respect to the back-gate voltage at charge neutrality, V_0. Details of tip functionalization are described in Supplementary Section 2.

Data availability

The data that support the findings of this study are available from the corresponding author upon reasonable request.

Additional information

Publisher's note: Springer Nature remains neutral with regard to jurisdictional claims in published maps and institutional affiliations.

References

1. Castro Neto, A. H., Guinea, F., Peres, N. M. R., Novoselov, K. S. & Geim, A. K. The electronic properties of graphene. *Rev. Mod. Phys.* **81**, 109–162 (2009).
2. Cheianov, V. V., Fal'ko, V. & Altshuler, B. L. The focusing of electron flow and a Veselago lens in graphene p–n junctions. *Science* **315**, 1252–1255 (2007).
3. Katsnelson, M. I., Novoselov, K. S. & Geim, A. K. Chiral tunnelling and the Klein paradox in graphene. *Nat. Phys.* **2**, 620–625 (2006).
4. Williams, J. R., Low, T., Lundstrom, M. S. & Marcus, C. M. Gate-controlled guiding of electrons in graphene. *Nat. Nanotech.* **6**, 222–225 (2011).
5. Lee, G. H., Park, G. H. & Lee, H. J. Observation of negative refraction of Dirac fermions in graphene. *Nat. Phys.* **11**, 925–929 (2015).
6. Chen, S. *et al.* Electron optics with p–n junctions in ballistic graphene. *Science* **353**, 1522–1525 (2016).
7. Wu, J. S. & Fogler, M. M. Scattering of two-dimensional massless Dirac electrons by a circular potential barrier. *Phys. Rev. B* **90**, 235402 (2014).
8. Heinisch, R. L., Bronold, F. X. & Fehske, H. Mie scattering analog in graphene: lensing, particle confinement, and depletion of Klein tunneling. *Phys. Rev. B* **87**, 155409 (2013).
9. Pomeranchuk, I. & Smorodinsky, J. On the energy levels of systems with Z >1/137. *J. Phys. USSR* **9**, 97–100 (1945).
10. Shytov, A. V., Katsnelson, M. I. & Levitov, L. S. Atomic collapse and quasi-Rydberg states in graphene. *Phys. Rev. Lett.* **99**, 246802 (2007).
11. Wang, Y. *et al.* Observing atomic collapse resonances in artificial nuclei on graphene. *Science* **340**, 734–737 (2013).
12. Mao, J. *et al.* Realization of a tunable artificial atom at a supercritically charged vacancy in graphene. *Nat. Phys.* **12**, 545–549 (2016).
13. Luican-Mayer, A. *et al.* Screening charged impurities and lifting the orbital degeneracy in graphene by populating Landau levels. *Phys. Rev. Lett.* **112**, 036804 (2014).
14. Rayleigh, L. CXII. The problem of the whispering gallery. *Philos. Mag. Ser. 6* **20**, 1001–1004 (1910).
15. Zhao, Y. *et al.* Creating and probing electron whispering-gallery modes in graphene. *Science* **348**, 672–675 (2015).
16. Matsko, A. B. & Ilchenko, V. S. Optical resonators with whispering-gallery modes-part I: basics. *IEEE J. Sel. Top. Quantum Electron.* **12**, 3–14 (2006).
17. Rickhaus, P. *et al.* Ballistic interferences in suspended graphene. *Nat. Commun.* **4**, 2342 (2013).
18. Lee, J. *et al.* Imaging electrostatically confined Dirac fermions in graphene quantum dots. *Nat. Phys.* **12**, 1032–1036 (2016).
19. Gutierrez, C., Brown, L., Kim, C. J., Park, J. & Pasupathy, A. N. Klein tunnelling and electron trapping in nanometre-

scale graphene quantum dots. *Nat. Phys.* **12**, 1069–1075 (2016).

20. Ghahari, F. *et al.* An on/off Berry phase switch in circular graphene resonators. *Science* **356**, 845–849 (2017).

21. Morgenstern, M. Scanning tunneling microscopy and spectroscopy of graphene on insulating substrates. *Phys. Status Solidi B* **248**, 2423–2434 (2011).

22. Andrei, E. Y., Li, G. & Du, X. Electronic properties of graphene: a perspective from scanning tunneling microscopy and magnetotransport. *Rep. Prog. Phys.* **75**, 056501 (2012).

23. Fogler, M. M., Novikov, D. S. & Shklovskii, B. I. Screening of a hypercritical charge in graphene. *Phys. Rev. B* **76**, 233402 (2007).

24. Requist, R. *et al.* Metallic, magnetic and molecular nanocontacts. *Nat. Nanotech.* **11**, 499–508 (2016).

25. Cui, L. *et al.* Quantized thermal transport in single-atom junctions. *Science* **355**, 1192–1195 (2017).

26. Ovdat, O., Mao, J., Jiang, Y., Andrei, E. Y. & Akkermans, E. Observing a scale anomaly in graphene: a universal quantum phase transition. *Nat. Commun.* Preprint at http://arXiv:1701.04121 (15 January 2017).

27. Grushina, A. L., Ki, D.-K. & Morpurgo, A. F. A ballistic pn junction in suspended graphene with split bottom gates. *Appl. Phys. Lett.* **102**, 223102 (2013).

28. Oksanen, M. *et al.* Single-mode and multimode Fabry–Pérot interference in suspended graphene. *Phys. Rev. B* **89**, 121414 (2014).

29. Luican, A., Li, G. & Andrei, E. Y. Scanning tunneling microscopy and spectroscopy of graphene layers on graphite. *Solid State Commun.* **149**, 1151–1156 (2009).

30. Lu, C.-P. *et al.* Local, global, and nonlinear screening in twisted double-layer graphene. *Proc. Natl Acad. Sci. USA* **113**, 6623–6628 (2016).

31. Jiang, Y. *et al.* Visualizing strain-induced pseudomagnetic fields in graphene through an hBN magnifying glass. *Nano Lett.* **17**, 2839–2843 (2017).

32. Li, G., Luican, A. & Andrei, E. Y. Self-navigation of a scanning tunneling microscope tip toward a micron sized sample. *Rev. Sci. Instrum.* **82**, 073701 (2011).

Acknowledgements

The authors acknowledge funding provided by DOE-FG02-99ER45742 (STM/STS) and NSF DMR 1708158 (fabrication). Theoretical work was supported by ESF-EUROCORES-EuroGRAPHENE, FWO-VI and the Methusalem program of the Flemish government.

Author information

Yuhang Jiang, Jinhai Mao & Dean Moldovan
These authors contributed equally to this work.

Affiliations

Department of Physics and Astronomy, Rutgers University, 136 Frelinghuysen Road, Piscataway, New Jersey 08855, USA
Yuhang Jiang, Jinhai Mao, Guohong Li & Eva Y. Andrei

Departement Fysica, Universiteit Antwerpen, Groenenborgerlaan 171, B-2020 Antwerpen, Belgium
Dean Moldovan, Massoud Ramezani Masir & Francois M. Peeters

Department of Physics, University of Texas at Austin, Austin, Texas 78712, USA
Massoud Ramezani Masir

Advanced Materials Laboratory, National Institute for Materials Science, 1-1 Namiki, Tsukuba 305-0044, Japan
Kenji Watanabe & Takashi Taniguchi

Contributions

Y.J., J.M. and E.Y.A. conceived the work and designed the research strategy. Y.J. and J.M. performed the experiments, analysed data and wrote the paper. G.L. built the STM. D.M., M.R.M. and F.M.P. carried out the theoretical work. K.W. and T.T. contributed the boron nitride. E.Y.A. directed the project, analysed the data and wrote the paper.

Competing interests

The authors declare no competing financial interests.

Corresponding author

Correspondence to Eva Y. Andrei.

Supplementary information

PDF files

1. Supplementary information
   Supplementary information

Rights and permissions

To obtain permission to re-use content from this article visit RightsLink.

Nature Nanotechnology ISSN 1748-3395 (online)

SPRINGER NATURE

© 2018 Macmillan Publishers Limited, part of Springer Nature. All rights reserved.